Modeling and characterization of irreversible switching and viscosity phenomena in perpendicular exchange-spring Fe-FePt bilayers

R. Pellicelli,[1] C. Pernechele,[1] M. Solzi,[1] M. Ghidini,[1] F. Casoli,[2] and F. Albertini[2]
[1]*Dipartimento di Fisica e CNISM, Università di Parma, Via G. P. Usberti 7/A, 43100 Parma, Italy*
[2]*Istituto IMEM-CNR, Parco Area delle Scienze 37/A, 43010 Parma, Italy*
(Received 29 April 2008; published 24 November 2008)

A numerical model has been developed for simulating magnetic domain configurations, remanence, and viscosity curves in systems with strong perpendicular anisotropy and strong disorder, starting from internal switching field distributions for pinning and nucleation processes in the slow dynamics regime. In the considered systems, the domains expand in a percolationlike manner and domain configuration displays fractal properties. The simulations show that even in the case of pinning not governed by nucleation an abrupt avalanche propagation of reversed domains occurs. It is moreover evidenced that a decrease of viscosity coefficients can coexist with lowered energy barrier heights. The model has been applied to perpendicular FePt thin films with granular morphology and corresponding exchange-coupled Fe/FePt bilayers, by exploiting magnetic force microscopy, dc demagnetization (DCD), isothermal remanence, and viscosity data. The comparison between magnetic viscosity phenomena in thin films and exchange-coupled bilayers has been achieved by the definition of an adimensional viscosity coefficient. The addition of the Fe layer causes a decrease of the maximum viscosity coefficient, thus demonstrating that viscosity measures can be utilized to verify the coupling of hard/soft layers. From experiments it is inferred that our samples are mainly influenced by the pinning energy barrier law, the linearity of which allows reconstructing universal viscosity curves starting from DCD data. The calculated activation volumes are comparable to the average grain volume of the FePt layer. The obtained results also demonstrate that the addition of the Fe layer leads to a widening and a shift to lower fields of the pinning field distribution, determining a decrease of both the maximum viscosity and the pinning energy barrier heights and an increase of the demagnetizing effective field.

DOI: 10.1103/PhysRevB.78.184434 PACS number(s): 75.60.Lr, 75.60.Jk, 75.70.Cn, 75.50.Ss

I. INTRODUCTION

Magnetic thin films with perpendicular anisotropy and exchange-coupled hard/soft systems are attracting considerable attention for their phenomenology, concerning in particular magnetization reversal process, domain configuration, and magnetization dynamics.[1–4] Moreover, the study and the modeling of irreversible magnetization processes represent a key objective for the understanding of the relationship between microstructure and magnetic behavior of real systems. In this context we propose a numerical model which allows the simulation of irreversible processes in the slow dynamics regime for magnetic two-dimensional systems that combine strong perpendicular anisotropy and strong disorder. In particular, we consider systems in which the reversal process involves very few nucleation events while the subsequent domain-wall propagation process is controlled by the structural disorder, corresponding to the presence of pinning centers with a random distribution of energy barriers. In magnetic systems of nanometric thickness, the dipolar interactions cannot play their usual role which would lead to periodic or dendritic patterns.[2,5] Accordingly, the magnetic reversed phase expands in a percolationlike manner due to the strong disorder.[5] Domain configurations show the scale invariance of fractal geometries characterized by large unreversed areas within the percolating cluster,[2] although at very large scales there may be enough nucleation centers to lead to more homogeneous and thus nonfractal patterns. In order to describe the above phenomenology we have developed a numerical model based on a statistical approach. In this model we consider the system as composed of identical hysteretic switching units characterized by proper distributions of internal switching fields both for nucleation and pinning processes. The simulations are utilized in order to reproduce dc demagnetization (DCD) and isothermal remanence (IRM) curves, and viscosity curves as well as domain configurations.

The model has been applied to exchange-coupled Fe/FePt bilayers with different soft layer thickness corresponding to three different magnetic behaviors: hard single layer, rigid magnet, and exchange-spring bilayers (see Refs. 6 and 7 for details). The 10 nm epitaxially grown FePt hard component, which is really the same in all the samples, is characterized by strong perpendicular anisotropy and granular morphology. Therefore, these systems are characterized by intergrain exchange coupling together with a feeble dipolar interaction due to the very low thickness.[5,8] The observed phenomenology can be considered analogous to that of percolated perpendicular media.[9,10] We expect that the presence of a soft coupled Fe layer influences both dipolar and exchange intergrain interactions, in addition to the effects of the exchange-coupling between hard and soft layers. Besides measurement of remanence and viscosity curves as well as magnetic force microscopy (MFM) imaging, a thorough magnetometric characterization is given also taking into account the effect of temperature in the range 100–300 K. With the aim of clarifying the comparison of magnetic viscosity measurements between the bilayers and the corresponding hard single layer we have defined an adimensional viscosity coefficient.

II. EXPERIMENTAL RESULTS

A series of equivalent 10 nm thick FePt hard layers with perpendicular anisotropy was deposited by rf sputtering on MgO (100) single crystals (the details are reported in Ref. 11). Two different soft Fe layers with nominal thickness 2 and 3.7 nm were also deposited at room temperature on the previously realized FePt layers under the same sputtering conditions.[12] The FePt layer morphology and magnetic domain configurations were studied by atomic force microscopy (AFM) and MFM, performed in tapping mode by a Dimension 3100 scanning probe microscope equipped with a Nanoscope IVa controller (Veeco Instruments). The hysteresis loops and magnetic viscosity curves in the perpendicular configuration were measured by means of a superconducting quantum interference device (SQUID) magnetometer (MPMSXL-5 Quantum Design) in the range of 100–300 K. An alternating gradient force magnetometer (AGFM) has also been utilized for room-temperature measurement of recoil, remanence, and viscosity curves.

A. Fe/FePt exchange-coupled bilayers

According to the definitions of different regimes given in a previously developed micromagnetic model,[7] the 2 nm Fe bilayer behaves as a rigid magnet (RM) until the occurrence of irreversible switching processes [see Fig. 1(b)] while the 3.7 nm Fe sample displays a reversible portion of the demagnetizing curve [see Fig. 1(c)], which is typical of an exchange spring (ES) magnet. It has to be noted that in the case of ES bilayer, the presence of the reversible portion in the demagnetizing curve is a necessary but not sufficient condition for demonstrating the effective coupling between the phases, as this feature is displayed in both coupled and fully decoupled systems. However, we have demonstrated[7] that the nucleation field H_{c1}, corresponding to the start of magnetization deviation from the saturated state (see Fig. 2), is a useful parameter for discriminating the presence of an effective coupling. Thus, we compared the 3.7 nm Fe bilayer to a fully decoupled sample constituted by the simple superposition of the FePt hard phase and a 3.7 nm Fe film directly deposited on MgO. The room-temperature hysteresis loops (with the field applied perpendicular to the film plane) reported in Fig. 2 show that the nucleation field for the decoupled system coincides with the demagnetizing field H_d of the saturated Fe layer and the coercive field H_c corresponds to the one measured for the FePt layer, differently from the bilayer, thus confirming its exchange-spring nature. In the case of the 2 nm Fe bilayer, the RM behavior down to negative fields is an indication of the effectiveness of the exchange coupling between hard and soft phases.

B. Domain structure and hysteresis loops

The observed morphology in the FePt layer [see Fig. 3(a)] is constituted of grains with average size in agreement with TEM observations[11] (15–25 nm lateral size). The MFM imaging of the magnetization configuration on the demagnetizing curve for the FePt film was performed by applying, after positive saturation, a particular reverse field and then promptly reducing it to zero with the aim of freezing the reversal process.[2,13] Figure 3(b) displays the magnetic domain configuration for a reverse field $H=3.5$ kOe below coercivity. In particular we observe that the domain structure turns out to be of fractal type, as typical of thin films with low dipolar effects.[2,5] This pattern is characteristic of a reversal process occurring by the nucleation of a few small reversed domains followed by their expansion through the switching of small regions with local pinning fields distributed over a rather wide field range. Therefore, the disorder seems to be the main parameter governing this pinning-type reversal process.

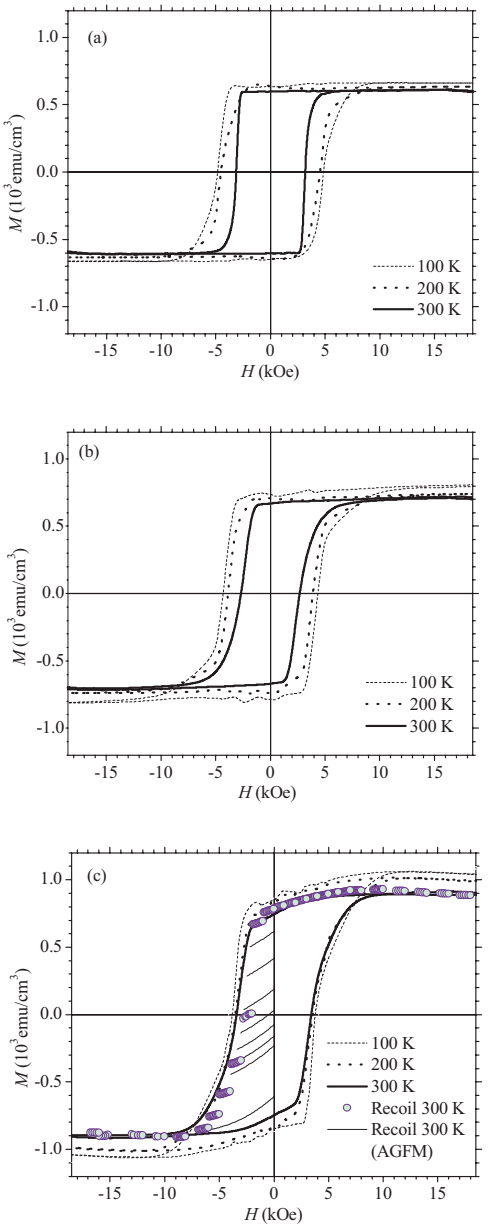

FIG. 1. (Color online) Hysteresis loops, measured by the SQUID magnetometer, (a) for the FePt (10 nm), (b) for the Fe (2 nm)/FePt (10 nm), and (c) for the Fe (3.7 nm)/FePt (10 nm) samples in the temperature range 100–300 K; SQUID (open circles) and AGFM (thin solid lines) room-temperature recoil curves for the Fe (3.7 nm)/FePt (10 nm) bilayer are also reported in (c).

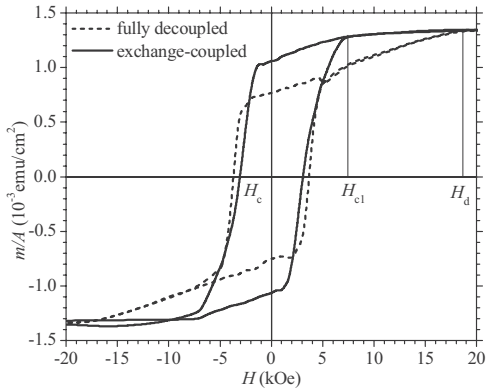

FIG. 2. Room-temperature hysteresis loops for the exchange-coupled and the fully decoupled Fe (3.7 nm)/FePt (10 nm) bilayer: H_{c1} and H_c are the nucleation and the coercive fields, respectively, of the exchange-coupled bilayer, while H_d is the nucleation field of the fully decoupled bilayer. The vertical axis reports the magnetic moment per unit area.

The hysteresis loops are reported in Figs. 1(a)–1(c) for the 10 nm FePt film, the 2 and 3.7 nm Fe bilayers, respectively. The loops of the FePt film and of the 2 nm Fe bilayer show a high squareness which is almost constant all over the investigated temperature range. The square hysteresis loop of FePt layer together with the initial magnetization curve (measured at room temperature and reported in Ref. 14) confirms that the magnetization reversal occurs by domain-wall depinning.[5,15] The remanence ratio of the 3.7 nm Fe bilayer is lower compared to the other samples (M_r/M_s is of the order of 0.8) as a marked nucleation field appears in the first quadrant due to demagnetizing effects.[7] The room-temperature recoil curves measured for this sample [also reported in Fig. 1(c)] confirm the occurrence of a completely reversible portion of the demagnetizing curve starting from the nucleation field until the field corresponding to the onset of irreversible processes is reached. In Table I the most important magnetic parameters of the samples (coercive field H_c, saturation magnetization M_s, and first-order uniaxial magnetocrystalline anisotropy constant K_a) are reported as a function of temperature.

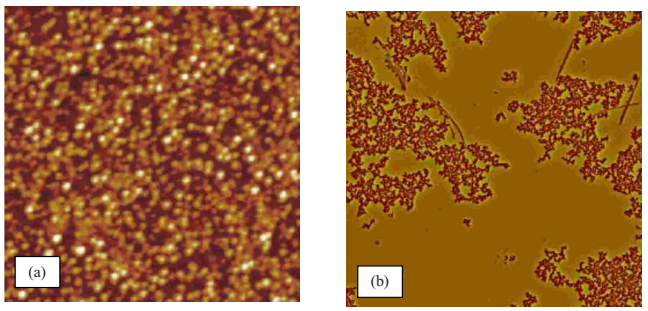

FIG. 3. (Color online) Scanning probe microscopy observations of the FePt (10 nm) film. (a) Topographical AFM image (0.8 $\times 0.8$ μm^2). (b) MFM domain configuration image (50 $\times 50$ μm^2) in the remanent state after application of a reverse magnetic field of 3.5 kOe.

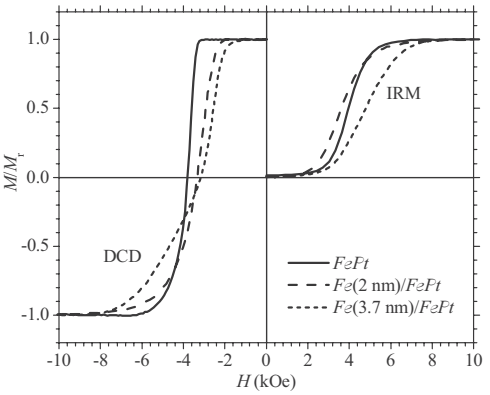

FIG. 4. Room-temperature normalized DCD and IRM curves, measured by the AGFM, for the FePt (10 nm) film and the Fe (2 nm)/FePt (10 nm) and the Fe (3.7 nm)/FePt (10 nm) bilayers.

C. Remanence and viscosity measurements

In a DCD measurement, a reverse constant magnetic field H is suddenly applied after positive saturation, then the field is rapidly reduced to zero and the remanent magnetization is detected. A similar procedure is adopted for IRM measurements, with the difference that the starting point is the dc demagnetized state and the applied field is usually positive. The remanence curves are reported (normalized to the remanent magnetization) in Fig. 4 for all the samples. It should be noted that the addition of a Fe layer markedly modifies both the DCD and IRM curves: on increasing Fe thickness, the field corresponding to the onset of irreversible processes is reduced in the DCD curves while the field range involved in the irreversible phenomena increases both in the DCD and IRM curves.

In a typical viscosity experiment, a reverse constant magnetic field H near the coercivity is applied after positive saturation under isothermal conditions and the magnetization M is detected as a function of time t. A general way to quantify the magnetic viscosity is to utilize the viscosity coefficient $S=-dM/d\ln t$. The investigation of the influence of the exchange-coupled soft layer on the viscosity processes of the hard FePt layer requires a comparison between heterogeneous systems. However, a problem of meaning arises which affects this comparison. A simple example is that of a perpendicular fully decoupled bilayer in which the soft layer is not involved in viscosity phenomena. If one assumes as the reference volume for the calculation of viscosity coefficient that of the whole system, paradoxically a lower S value would be deduced in comparison to the isolated hard layer. Analogously, two homogeneous systems which relax their magnetization starting from the saturated state and characterized by distinct saturation magnetization but equal half life have different viscosity coefficients. A viable criterion for comparing different systems could be to take into account the variation of the total fraction P of noninverted material. If we assume, as usual in literature, that our system is constituted of elementary units that can irreversibly switch their magnetic moment, P can be expressed at a given field H as

TABLE I. Measured magnetic features of the FePt (10 nm) film, the Fe (2 nm)/FePt (10 nm), and the Fe (3.7 nm)/FePt (10 nm) bilayers as a function of temperature (where K_a is first-order uniaxial magnetocrystalline anisotropy constant, M_s the saturation magnetization, M_r the remanence magnetization, and H_c the coercive field).

T (K)	K_a (erg/cm^3)	M_s (emu/cm^3)	H_c (kOe)	M_s (emu/cm^3)	H_c (kOe)	M_s (emu/cm^3)	M_r (emu/cm^3)	H_c (kOe)
	FePt			Fe (2 nm)		Fe (3.7 nm)		
100	2.0×10^7	662	4.83	796	4.27	1066	917	3.79
200	1.5×10^7	630	4.45	738	3.76	1008	834	3.59
300	1.4×10^7	624	3.67	709	3.06	890	690	3.43

$$P = \frac{1}{2} + \frac{M_{\text{irr}}}{2M_r}, \tag{1}$$

where M_r being the remanent magnetization and M_{irr} the irreversible component of magnetization (i.e., the value of magnetization after a sudden reduction to zero of the applied reverse field). The above equation reflects the fact that $-M_r \leq M_{\text{irr}} \leq M_r$ and it is valid if the irreversible switching of the units only occurs in the second quadrant of the hysteresis loop, as in the case of our systems. On the basis of Eq. (1) one can define an adimensional viscosity coefficient

$$s = -\frac{dP}{d\ln t} = \frac{S}{2M_r}. \tag{2}$$

Therefore, we will consider for all the samples the time evolution of the irreversible component of perpendicular magnetization normalized to remanent magnetization. In the case of the 3.7 nm Fe bilayer, for which there is a non-negligible reversible contribution, we have utilized the AGFM recoil curves [see Fig. 1(c)] to deduce the irreversible component.

Due to the typical SQUID measurement time for each point, the time required to reach the target field and the presence of a nonlinear drift in the sensor, for our analysis we only considered the experimental points for $t > 400$ s. Moreover, the measurements were made over a total time in the range of $t_{\max} = 90-300$ min. We have also utilized the AGFM for measuring at room temperature the time dependence on short timescales and with rapid field settings. Due to the possible presence of drift in the resonant actuator of this instrument, we limited the viscosity measurements to a maximum time of the order of $t_{\max} = 1000$ s. Moreover we were forced to consider the curves only for times $t > 20$ s [i.e., $\ln(t) > 3$], so that the uncertainty on the time t_0 required for the initial field setting has a negligible effect on the shape of the curves on a logarithmic scale. We can notice that the curves are not linear on a logarithmic time scale (see Fig. 5 for the FePt sample), as frequently observed in the literature. However, on limiting the time interval to $t > 400$ s the curves appear reasonably linear thus allowing to deduce the adimensional viscosity coefficient $s(H,T)$. A comparison between the $s(H)$ curves under isothermal condition for the FePt sample and the bilayers is reported in Fig. 6(a) where the effect of the addition of the soft layer is to reduce both the maximum s value and the corresponding field value. Moreover a broadening of the $s(H)$ curve is observed. These results are not compatible with a bilayer in which Fe is fully decoupled from FePt, since a decoupled soft layer would not contribute to the system viscosity, in particular near the FePt coercivity. Even if we calculate the viscosity coefficient s on the basis of the FePt layer volume, we obtain a $s(H)$ curve evidently modified in comparison to the FePt film. This confirms therefore the existence of a real exchange coupling between hard and soft layers in the bilayers. As an important general consequence of the above analysis, we clearly demonstrated that viscosity measurements can be a useful mean to discriminate the occurrence of exchange coupling.

The temperature evolution of $s(H,T)$ curves is displayed in Fig. 6(b) for the case of FePt film. It is found that on decreasing temperature the s maximum value is strongly reduced while the corresponding field increases toward negative values and the $s(H)$ curve broadens. A similar behavior has been found in the case of the Fe/FePt bilayers.

III. MODELING OF IRREVERSIBLE SWITCHING AND VISCOSITY

A. Numerical model

In order to describe the irreversible magnetization reversal process in systems where it is mainly driven by the disorder, we have developed a numerical model based on a statistical approach. The simulated system is represented as a

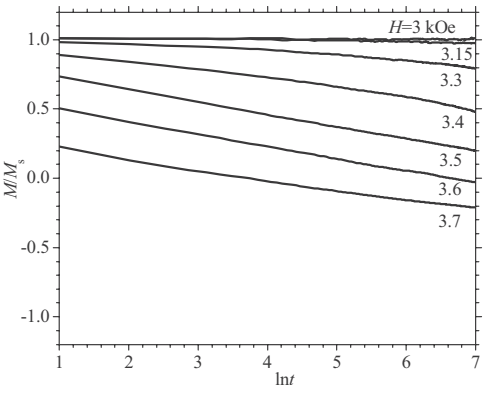

FIG. 5. Normalized viscosity curves with different external fields, measured by the AGFM at room temperature for the FePt (10 nm) film.

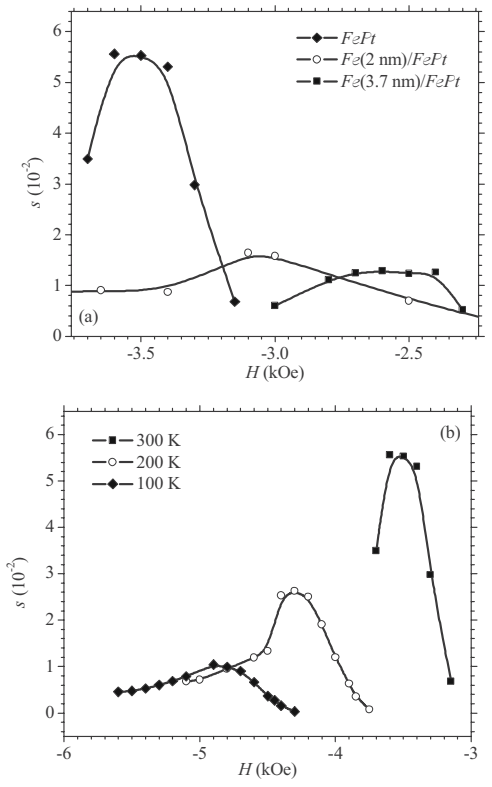

FIG. 6. Field dependence of the adimensional viscosity coefficient $s(H)$ as defined by Eq. (2): (a) for the FePt (10 nm) film and the Fe (2 nm)/FePt (10 nm) and the Fe (3.7 nm)/FePt (10 nm) bilayers at 300 K; (b) for the FePt (10 nm) film at different temperatures. The lines are guides to the eyes.

periodic structure composed of rectangular grids of elementary units that can irreversibly switch their magnetic moment by means of two specific and subsequent mechanisms:[16] nucleation of reverse domains and domain-wall motion governed by pinning process. Each of these mechanisms is in general characterized by a proper switching field distribution (SFD). Some particular cases can occur in real systems:[17] (i) *pure pinning*, when the nucleation of a small fraction of units (with a negligible direct contribution to reversal of magnetization) occurs for switching fields (SFs) lower than the pinning SFs (magnetization reversal exclusively controlled by the pinning SFD); (ii) *pinning+nucleation*, when the nucleation and the pinning SFDs have appreciable values in overlapped field ranges (pinning governed by nucleation). A different case is that of *pure nucleation*, occurring when the pinning is not involved in the magnetization reversal process.

In this treatment we consider the domain wall simply as the boundary between reversed and nonreversed regions, thus intending the domain-wall motion as the propagation of the reversed magnetization from a reversed unit to the adjacent ones. In the case of pinning, the units with lower SF can be involved in the process suddenly after units with larger SF due to the fact that a particular unit is not implicated until it is reached by an expanding domain wall. As a consequence, the total effective volume involved in a single switching event is in general a variable multiple of the elementary unit volume.

The considered SFDs are expressed in terms of the internal field H_i, which is the sum of applied, dipolar, exchange, and anisotropy fields acting on a single elementary unit. Magnetic forces which are proportional to the net magnetization of the system, on average, are represented by introducing an effective field $H_{\text{eff}}=4\pi d_{\text{eff}}M$, in which the *effective-field factor* d_{eff} tends to zero in the case of small film thicknesses due to the reduced efficiency of dipolar interactions.[5,8,18]

The simulations have been performed to deduce the DCD and IRM curves, where the simulated quantity is the irreversible component of magnetization $M_{\text{irr}}(H)$, the viscosity curves $M_{\text{irr}}(t)$, and the related domain configurations. In the model, the switchable units are inserted in a queue organized as a binary search tree ordered by the switching field or the switching time value. In the case of viscosity curves, the switching times are calculated by utilizing the Arrhenius law $\tau=\tau_0 \exp(E/k_BT)$, which expresses the mean relaxation time τ of the units characterized by energy barriers of height E. The attempt time τ_0 typically assumes values in the range $10^{-12}-10^{-8}$ s.[19] Moreover, one has to assume a suitable expression for the energy barrier $E(H_i,H_{\text{swi}})$, in which H_{swi} is the internal switching field of the interested unit. The viscosity curves are generated starting from configurations belonging to the DCD curves. In the performed simulations, the considered values of the applied field are sufficiently far from zero so that one can neglect the probability of back switching of the inverted units to their original state.

In the particular case of pure pinning, the phenomenology of the reversal process fits the percolation theory,[20,2] at least in the case of a single nucleation center. Differently from Attané *et al.*,[2] we have considered both the case of site percolation[20] (a unique pinning SF assigned to each unit) and the case of bond percolation[20] (a different SF assigned to each link between a given unit and the four adjacent ones, even if in real systems these SFs are likely to be correlated). Furthermore, we have considered the influence of the nucleation SFD and of the effective field, and we have applied the model to simulate also remanence and viscosity curves.

B. Simulation of DCD and IRM remanence curves

The analysis of DCD and IRM curves can be in principle utilized to deduce the switching field distributions.[21] However, a direct correspondence between the remanence curves and the SFDs only exists in the case of a pure nucleation process. In the case of pinning process the switching of a unit due to a field increment could cause the avalanche switching of adjacent units with lower SFs. Moreover, the only units which modify their magnetic state on incrementing the field are those adjacent to already reversed units, while other nonadjacent and nonreversed units could exist with SFs in the same range of values, thus contributing to the SF distribution function but not to the remanence curve. In addition, the observed SF of a given unit is the minimum one among the SFs associated with the links toward the adjacent inverted units. To illustrate this point, numerical simulations have been performed on a 512×512 grid. Figures 7(a) and 7(b) display the comparison between the calculated DCD

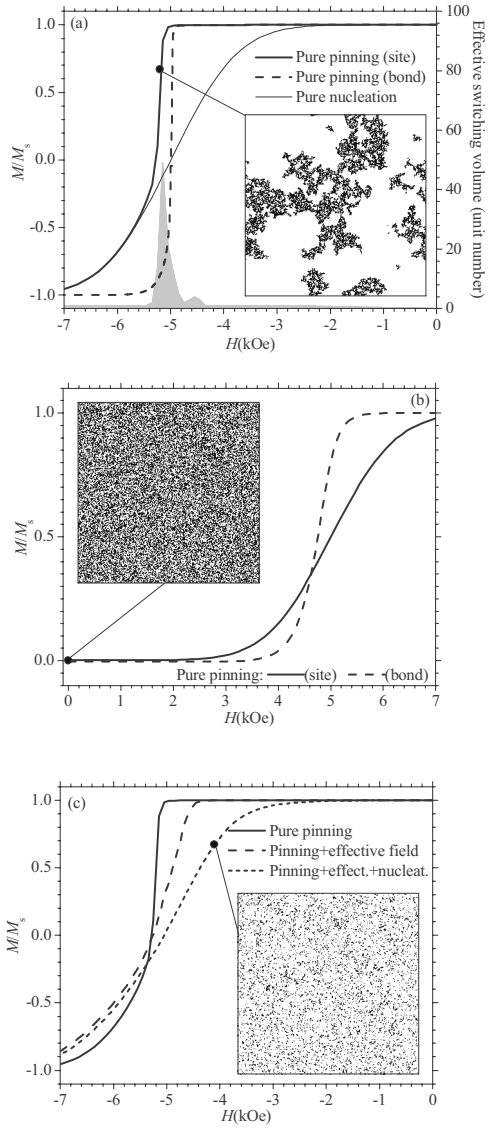

FIG. 7. Simulations obtained for different processes utilizing a 512×512 rectangular grid. (a) Comparison among normalized DCD curves for pure pinning in the case of site and bond percolation and pure nucleation; the boundary of the gray area represents the effective switching volume in terms of the number of switched units (right scale); inset shows the domain configuration in the state evidenced on the DCD curve. (b) Normalized IRM curves for pure pinning in the case of site and bond percolation; inset shows the domain configuration in the demagnetized state. (c) Comparison among normalized DCD curves for pure pinning with and without effective fields and pinning+nucleation with effective field; inset shows the domain configuration in the state evidenced on the DCD curve.

and IRM curves for pure pinning and pure nucleation processes. We have imposed $d_{\text{eff}}=0$ (which is equivalent to express the curves in terms of H_i instead of H) and we have adopted a Gaussian SFD with a mean value of 5 kOe and a standard deviation of 1 kOe. In order to activate the pure pinning phenomenon, the nucleation of a limited fraction (1×10^{-4}) of material has been imposed at low fields. The comparison evidences that, in the case of pure pinning with bond percolation, the SFD is not directly correlated with the

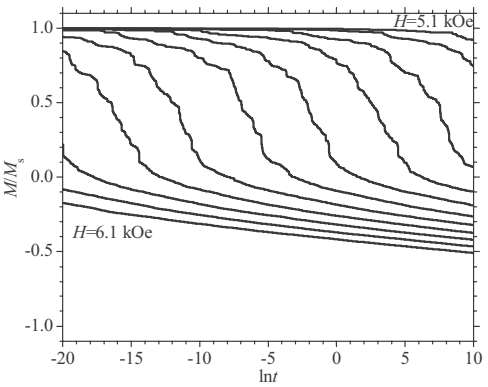

FIG. 8. Simulation of normalized viscosity curves, obtained for the case of a pure pinning process with uniform energy barrier distribution, in the field range 5.1–6.1 kOe with a 100 Oe field step.

remanence curves. However, if the SFs associated with a given unit coincide (site percolation), the IRM curve reproduces exactly the SFD, while the DCD curve tends to the SFD only for reverse fields greater than coercivity. The simulated DCD curve displays an abrupt magnetization reversal even if the magnetization reversal is not governed by the nucleation SFD.[17] The inset of Fig. 7(a) shows the simulated domain configuration corresponding to the indicated point on the DCD curve: it turns out to be a typical fractal-like pattern (the box counting fractal dimension is 1.71 and it tends to 2 when increasing the box size due to the contribution of nucleation). The effective switching volume is a multiple of the elementary unit volume and varies on the average in a nonrandom way, progressively increasing for fields lower than coercivity and then gradually reducing to the elementary unit volume.

The slope of DCD curves in the case of pure pinning is almost independent of the small fraction of nucleation centers. The inclusion of an effective field with $d_{\text{eff}}>0$ determines a lowering of the slope (if the DCD curves are expressed, as usual, in terms of external field) in the neighborhood of the coercivity,[17] while the domain configuration keeps its fractal nature. Figure 7(c) shows the DCD curve calculated in the case of pure pinning by assuming $d_{\text{eff}}=0.05$, $M_s=1000$ emu/cm^3, in comparison to the case $d_{\text{eff}}=0$. It has to be noted that for a pinning+nucleation process (Gaussian nucleation SFD with a mean value of 8 kOe and a standard deviation of 2 kOe, which determines a 10% nucleated units), a further reduction of slope of the DCD curve can be observed together with a more uniform look of the domain pattern [see inset of Fig. 7(c)]. Accordingly, the calculated fractal dimension tends rapidly to 2 when increasing the box size.

C. Viscosity with linear energy barrier law

Experiments reported in literature[5,15,22] show that for strongly disordered systems, the energy barrier often varies linearly with H_i so that $E=\alpha(H_{\text{swi}}-H_i)$. As an example, the simulated viscosity curves obtained starting from states of the ideal (that is, instantaneous) DCD curves for pure pinning and $d_{\text{eff}}=0$ are reported in Fig. 8 for a uniform pinning

SFD with values between 3 and 8 kOe and by assuming $\alpha = 2 \times 10^{-15}$ erg/Oe. One can observe that differently from the pure nucleation case, the viscosity curves show a typical nonlinear dependence on $\ln(t)$ even if the resulting energy barrier distribution is uniform. This fact is due to the variable effective switching volume typical of the pinning process.

In the case of a reversal driven by a predominant single process (pure pinning or pure nucleation), the magnetization under a constant reverse field H changes with time starting from the $M_{\mathrm{irr}}(H_{\mathrm{DCD}}=H)$ state of the DCD curve and it reproduces on average the configurations of the DCD curve which are characterized by increasing fields. As a consequence, when considering two viscosity curves for applied fields H and $H' > H$, all the switching events that occur in the H' curve starting from the initial configuration $M_{\mathrm{irr}}(H_{\mathrm{DCD}}=H')$ take place even in the H curve as soon as $M_{\mathrm{irr}} \geq M_{\mathrm{irr}}(H_{\mathrm{DCD}}=H')$. However, the times generated for the two curves on the basis of the Arrhenius law differ by a multiplicative factor $\exp[-\alpha_0(H'-H)/k_BT]$. Thus the times t and t' of corresponding events on the two viscosity curves are related by

$$\ln t' = \ln t - \frac{\alpha(H'-H)}{k_BT}. \tag{3}$$

In the case of pinning events, the above conclusion is true only if we chose the time origin for the H curve at the instant t^* at which the state $M_{\mathrm{irr}}(H_{\mathrm{DCD}}=H')$ is reached. However, the shape of the curve for $t \gg t^*$ is independent of this choice on a logarithmic scale. Moreover, t^* is typically very small in comparison to the delay t_0 due to the initial field setting of our viscosity measurements, since it is the sum of increasing switching times which start from values of the order of τ_0. The time shift property expressed by Eq. (3) remains valid even in the case of pure pinning with non-negligible effective field if reversible phenomena are absent. In the presence of a reversible component of magnetization characterized by approximately constant χ_{rev}, the energy barrier law remains unchanged provided that α is replaced by $\alpha' = (1 + 4\pi d_{\mathrm{eff}}\chi_{\mathrm{rev}})\alpha$.

As a first consequence of Eq. (3), the viscosity curves corresponding to different applied fields can be deduced from the others by a time shift on the logarithmic scale. This property reflects in an analogous field shift of the nonideal DCD curves

$$\Delta H = -\frac{k_BT(\ln t_0' - \ln t_0)}{\alpha_0}, \tag{4}$$

where t_0 and t_0' represent the measurement delay times of two DCD curves. The above equation can be justified considering that a DCD curve with a delay time t_0 consists of the magnetization states reached at time t_0 by the ideal viscosity curves for all the possible applied field values. As a second consequence of Eq. (3), the susceptibility and the viscosity coefficient of the ideal and nonideal DCD and viscosity curves in the same magnetization state M_{irr} are related by $dM_{\mathrm{irr}}/dH = -(a/k_BT)dM_{\mathrm{irr}}/d\ln t$. We deduce therefore an expression for the α constant

$$\alpha = -\frac{k_BT\dfrac{dM_{\mathrm{irr}}}{dH}}{\dfrac{dM_{\mathrm{irr}}}{d\ln t}} = \frac{k_BT\chi_{\mathrm{irr}}}{S}. \tag{5}$$

Moreover, the delayed viscosity curve under a given reverse field H can be obtained starting from the DCD curve $M_{\mathrm{irr}}(H_{\mathrm{DCD}})$ with the same delay time by using the field-to-time transformation

$$H_{\mathrm{DCD}} \rightarrow \ln t = \frac{\alpha}{k_BT}(H_{\mathrm{DCD}} - H). \tag{6}$$

From the above result, it can be deduced that a reduction of the SF values (and thus of the energy barrier heights) does not necessarily determine an increase of the maximum viscosity coefficient $S_{\max}$ of the system. The broadening of the SFD produces indeed a reduction of the maximum susceptibility and consequently of $S_{\max}$ (provided that the energy barrier field dependence does not change) even in the case of a SFs decrease. We can conclude that a simultaneous reduction of maximum viscosity and energy barrier heights can occur. The time shift property (3) of viscosity curves allows to virtually extend the curve for a given applied field measured over a limited time range, so achieving universal viscosity curves[15,23] varying over a much wider time interval.

On the basis of viscosity measurements one can estimate the size of the elementary unit by calculating the activation volume, which is generally expressed as[24,25] $V_{\mathrm{act}} = k_BT\chi_{\mathrm{irr}}/(SM_s)$, for applied fields above coercivity. Utilizing Eq. (5), then we deduce

$$V_{\mathrm{act}} = \frac{\alpha_0}{M_s}, \tag{7}$$

which is valid independently of the applied field value, in particular above coercivity. An alternative expression can be obtained from Eqs. (3) and (7) (see also Ref. 15)

$$V_{\mathrm{act}} = \frac{k_BT}{M_sH_f}, \tag{8}$$

in which the fluctuation field $H_f = -(dH/d\ln t)|_{M_{\mathrm{irr}}}$ appears.

IV. APPLICATION OF THE MODEL

The model has been applied with the aim of describing the essential features of the demagnetization and viscosity processes for the realized systems (see Sec. II). We have adopted the site percolation approach, as one can only observe the SFs of the links between units which are really involved in the reversal process, and we have deduced the information on the pinning SFD and the effective-field factor directly from the experimental remanence curves, assuming that the direct contribution of nucleation processes is rather small (pure pinning). We have imposed a fraction 1×10^{-5} of nucleation centers, as roughly deduced from the MFM pictures. We have calculated d_{eff} from the slopes of the experimental DCD curves in the region below coercivity, obtaining $d_{\mathrm{eff}}=0.04$, $d_{\mathrm{eff}}=0.09$, and $d_{\mathrm{eff}}=0.08$ for the FePt film, the 2

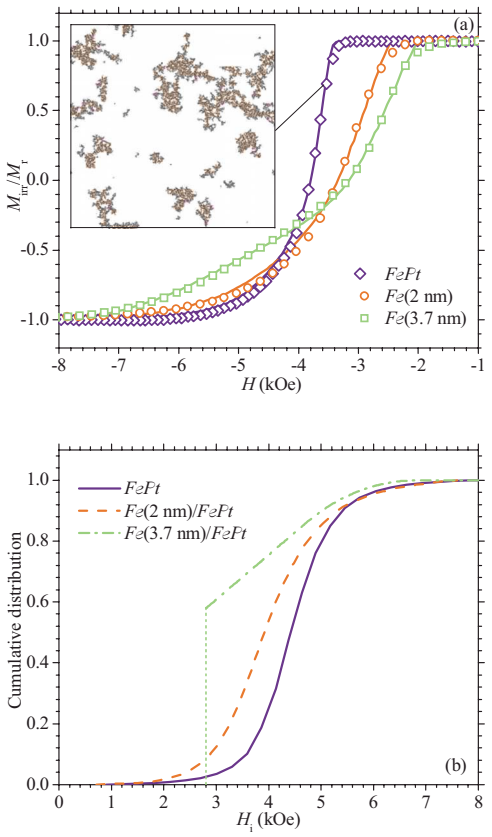

FIG. 9. (Color online) (a) Comparison between the room-temperature experimental (open symbols) and simulated (solid lines) normalized DCD curves, and (b) "true" pinning switching field distributions expressed in terms of internal field, for the FePt (10 nm) film and the Fe (2 nm)/FePt (10 nm) and the Fe (3.7 nm)/FePt (10 nm) bilayers. Inset: simulation on a 2500×2500 grid of the domain configuration (external reverse field $H=3.5$ kOe).

nm, and the 3.7 nm Fe bilayers, respectively. The comparison between the d_{eff} values suggests that a larger contribution of dipolar forces takes place in the bilayers. Furthermore, the small d_{eff} values imply the presence of a non-negligible exchange coupling between the grains of the samples.[18] Because the experimental DCD and IRM curves are affected by the viscosity phenomenon, they do not allow achieving the exact position of the SFDs on the switching field axis. In the case of the FePt film and the 2 nm Fe bilayer, the SFDs have been deduced directly from the experimental IRM curves (see Fig. 4) by expressing them in terms of internal field, with a shift toward lower fields of 0.2 and 0.3 kOe, respectively. In the case of the 3.7 nm Fe bilayer, the reversible component of magnetization, required to calculate the effective field, has been approximately expressed as $M_{\text{rev}} \cong -\chi_{\text{rev}} H$, having assumed a constant reversible susceptibility $\chi_{\text{rev}}=0.05$ emu cm^{-3} Oe^{-1}. Moreover, we have deduced the pinning SFD directly from the DCD curve for the useful field region above coercivity. Figure 9(a) displays the simulated DCD curves compared to the experimental ones.

With reference to the analysis of the viscosity experiments, we report in Fig. 10 (for $H=3.3$ kOe) the universal viscosity curve achieved for the FePt sample by applying the transformation (6) to the corresponding experimental DCD

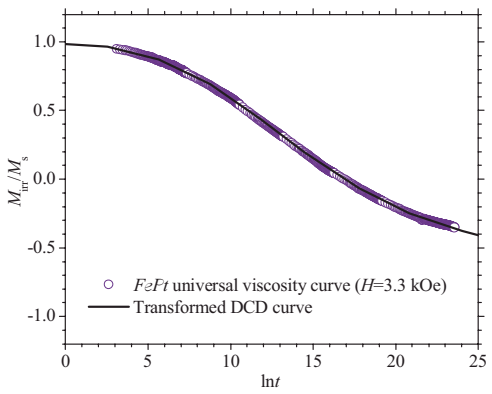

FIG. 10. (Color online) Room-temperature plot of the FePt (10 nm) universal viscosity curve compared to the corresponding DCD curve transformed by the $H \rightarrow \ln t$ substitution of Eq. (4).

curve, with $\alpha=1.25 \times 10^{-15}$ erg/Oe and imposing a delay time $t_0=20$ s (see Sec. II). The α constant has been evaluated for the three samples at the maximum viscosity field on the basis of Eq. (5), obtaining 1.3×10^{-15} erg/Oe, 1.3×10^{-15} erg/Oe, and 1.4×10^{-15} erg/Oe for the FePt film, the 2 nm, and 3.7 nm Fe bilayers, respectively. We can then conclude that the three systems are substantially characterized by the same energy barrier law. Afterward, the numerical model has been applied for the direct simulation of viscosity curves. The adopted approximate method for generating the delayed viscosity curves consisted in starting from the states of the ideal DCD curve at the simulation time $t=0$ s. This ideal DCD curve has to be calculated by utilizing the true SFDs, which in turn can be deduced by shifting the previously utilized SFDs toward larger fields (field shift H_0) in order to compensate for the viscosity effects on the remanence curves. The maximum viscosity curves for the FePt film and the 2 and the 3.7 nm Fe bilayers are reported in Fig. 11. In these simulations we have set $\alpha=1.25 \times 10^{-15}$ erg/Oe, $\tau_0=10^{-10}$ s, and $H_0=0.8$ kOe [as deduced from Eq. (4) by assuming $t_0' \cong 1$ s and $t_0 \cong \tau_0$].

The activation volume (7) turns out to be 0.6 and 0.5 times the average grain volume V_g for the FePt film and the

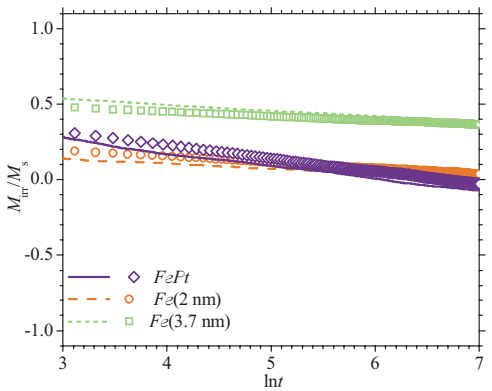

FIG. 11. (Color online) Room-temperature experimental (open symbols) and simulated (lines) maximum viscosity curves of the FePt (10 nm) film and the Fe (2 nm)/FePt (10 nm) and the Fe (3.7 nm)/FePt (10 nm) bilayers. The corresponding external reverse fields are 3.6, 3.1, and 2.5 kOe, respectively.

2 nm Fe bilayer, respectively. In the case of the 3.7 nm Fe bilayer, we have to consider that in general for the pinning process the theoretical activation volume roughly represents the volume of actually switched units only for large reverse field (see Sec. III). In this condition the Fe magnetization can be considered completely reversible and substantially lying in the film plane so that only FePt contributes to the perpendicular component of magnetization.[7] Then the activation volume of the bilayer is approximately the same as that of the FePt film. By applying relation (8) to the SQUID viscosity measurements performed on the FePt film, we have achieved $H_f=30$ Oe and $V_{\mathrm{act}}=0.7\ V_g$, in agreement with the AGFM measurements. Since the activation volumes turn out to be of the order of the average grain volume, it is reasonably to suppose that each grain acts as a single pinning center. The inset of Fig. 9(a) shows the simulation of domain configuration for the FePt film, with applied reverse field $H=3.5$ kOe. The adopted grid is 2500×2500 units, corresponding to a 50×50 $\mu\mathrm{m}^2$ area if one assumes that each elementary unit represents a single grain. The comparison with the MFM images reported in Fig. 3(b) for the same area and the same field allows concluding that the model based on pure pinning with non-negligible effective field is adequate to describe the observed phenomenology.

From the above results we can conclude that the presence of a Fe soft layer coupled to the hard one determines a widening and a simultaneous shift to lower fields of the pinning SFD [see Fig. 9(b)]. In addition, the Fe soft layer causes an increase of the effective-field factor d_{eff} as well as of the saturation magnetization and thus of the demagnetizing effective field in the saturated state, while the energy barrier law remains substantially unchanged. Therefore both the maximum viscosity and the pinning energy barrier heights turn out to be decreased.

Concerning the influence of temperature on both DCD and viscosity curves, it has to be underlined that besides the explicit contribution due to the thermal energy factor k_BT, an indirect role is played by the temperature dependence of the SFDs and of the parameters d_{eff}, τ_0, and α, which in turn depend on the intrinsic quantities A, K_a, and M_s. From Fig. 1 we can deduce that the DCD curves, and thus the SFDs, move toward larger reverse fields on decreasing temperature. If this effect was only due to the reduction of viscosity related to k_BT and affecting the experimental DCD curves, it would determine a shift $0.4\leq\Delta H\leq0.6$ kOe between 300 and 100 K [as deduced from Eq. (4) by assuming $t_0'\cong1$ s and $t_0\cong\tau_0$, where $10^{-12}\leq\tau_0\leq10^{-8}$ s], which is lower than that deduced from Fig. 1 and Table I ($\Delta H_c\cong1.16$ kOe and $\Delta H_c\cong1.21$ kOe for the FePt film and the 2 nm Fe bilayer, respectively). Analogously, for the FePt film the maximum viscosity coefficient between 300 and 100 K should increase by a factor of 3 instead of the observed factor 5.3 [see Fig. 6(b)].

V. CONCLUSIONS

We have developed a numerical model based on a statistical approach, aimed at simulating the irreversible switching of magnetization in the slow dynamics regime, thus allowing the calculation of remanence curves, domain configurations, and, once assumed a given energy barrier law, viscosity curves. The simulations have allowed demonstrating that an abrupt avalanche propagation of reversed domains occurs near coercivity even in the case of a process originating by a limited number of nucleation events at fields below the minimum pinning switching field (pinning not governed by nucleation). By applying the model to the simulation of viscosity curves we have evidenced that a decrease of viscosity coefficients, due to a widening of the switching field distribution, can coexist with a lowering of the energy barrier heights.

The model has been applied to the analysis of the magnetic behavior of perpendicular FePt thin films and exchange-coupled Fe/FePt bilayers. In order to allow the comparison of magnetic viscosity phenomena in different systems, we have defined an adimensional viscosity coefficient based on the time evolution of the fraction of unswitched material. We have demonstrated, by a direct comparison with a fully decoupled system, that the hard and soft phases of the bilayers are actually exchange coupled. Moreover, the addition of a coupled Fe layer to the FePt film has been shown to determine a decrease of the maximum viscosity coefficient, together with a widening and a shift toward lower fields of the field dependence of the adimensional viscosity coefficient. We have thus demonstrated that viscosity measurements can also be utilized to verify the actual coupling of hard/soft layers.

The DCD curves and the domain configurations of the three samples have been simulated assuming a non-negligible effective field. The analysis of experimental viscosity curves allows inferring that our samples are characterized by a linear energy barrier law for pinning, which is the same for the three systems. The linearity of energy barrier law implies the possibility of reconstructing universal viscosity curves, starting from the DCD measurements. The calculated switching volume for the three samples turns out to be comparable with the average grain volume of the FePt layer, thus suggesting that each FePt grain acts as a single pinning center. In summary, on the basis of the above results we can reasonably assert that the presence of a soft Fe layer exchange coupled to the FePt hard layer determines a widening and a shift to lower fields of the pinning switching field distribution, as well as an increase of the demagnetizing effective field. Therefore, being the energy barrier law the same for the three samples, both the maximum viscosity and the pinning energy barrier heights turn out to be decreased. As a final remark, we conclude that the effect of temperature on the DCD and viscosity measurements cannot be exclusively ascribed to the variation of the thermal energy factor.

ACKNOWLEDGMENTS

The present work has been supported by a PRIN Project entitled "Magnetization dynamics in artificial and self-assembling ferromagnetic nanostructures."

[1] H. Kronmüller and D. Goll, Physica B (Amsterdam) **403**, 237 (2008).
[2] J. P. Attané, Y. Samson, A. Marty, J. C. Toussaint, G. Dubois, A. Mougin, and J. P. Jamet, Phys. Rev. Lett. **93**, 257203 (2004).
[3] D. Suess, J. Fidler, G. Zimanyi, T. Schrefl, and P. Visscher, Appl. Phys. Lett. **92**, 173111 (2008).
[4] R. H. Victora, M. Kapoor, A. K. Hamre, and S. Hernandez, J. Appl. Phys. **103**, 07F544 (2008).
[5] J. Ferré, in *Spin Dynamics in Confined Magnetic Structures I*, Topics in Applied Physics Vol. 83, edited byB. Hillebrands and K. Ounadjela (Springer-Verlag, Berlin, 2002), p. 127.
[6] G. Asti, M. Solzi, M. Ghidini, and F. M. Neri, Phys. Rev. B **69**, 174401 (2004).
[7] G. Asti, M. Ghidini, R. Pellicelli, C. Pernechele, M. Solzi, F. Albertini, F. Casoli, S. Fabbrici, and L. Pareti, Phys. Rev. B **73**, 094406 (2006).
[8] U. Nowak, J. Heimel, T. Kleinefeld, and D. Weller, Phys. Rev. B **56**, 8143 (1997).
[9] J. Zhu and Y. Tang, J. Appl. Phys. **99**, 08Q903 (2006).
[10] M. T. Rahman, N. N. Shams, Y. Wu, C. Laia, and D. Suess, Appl. Phys. Lett. **91**, 132505 (2007).
[11] F. Casoli, F. Albertini, L. Pareti, S. Fabbrici, L. Nasi, C. Bocchi, and R. Ciprian, IEEE Trans. Magn. **41**, 3223 (2005).
[12] F. Casoli, F. Albertini, S. Fabbrici, C. Bocchi, L. Nasi, R. Ciprian, and L. Pareti, IEEE Trans. Magn. **41**, 3877 (2005).
[13] J. Pommier, P. Meyer, G. Pénissard, J. Ferré, P. Bruno, and D. Renard, Phys. Rev. Lett. **65**, 2054 (1990).
[14] F. Casoli, L. Nasi, F. Albertini, S. Fabbrici, C. Bocchi, F. Germini, P. Luches, A. Rota, and S. Valeri, J. Appl. Phys. **103**, 043912 (2008).
[15] C. S. Brown, J. W. Harrell, and S. Matsunuma, J. Appl. Phys. **100**, 053910 (2006).
[16] M. Mansuripur, J. Appl. Phys. **63**, 5809 (1988).
[17] T. Thomson and K. O'Grady, J. Phys. D **30**, 1566 (1997).
[18] R. J. M. van de Veerdonk, X. W. Wu, R. W. Chantrell, and J. J. Miles, IEEE Trans. Magn. **38**, 1676 (2002).
[19] G. Bertotti, *Hysteresis in Magnetism* (Academic, San Diego, 1998).
[20] A. Bunde and S. Havlin, in *Fractals and Disordered Systems*, edited by A. Bunde and S. Havlin (Springer-Verlag, Berlin, 1991), Chap. 2.
[21] T. Thomson, K. O'Grady, and G. Bayreuther, J. Phys. D **30**, 1577 (1997).
[22] A. Lyberatos, J. Earl, and R. W. Chantrell, Phys. Rev. B **53**, 5493 (1996).
[23] S. D. Brown, R. Street, R. W. Chantrell, P. W. Haycock, and K. O'Grady, J. Appl. Phys. **79**, 2594 (1996).
[24] L. Néel, J. Phys. Radium **12**, 339 (1951).
[25] P. Gaunt, Philos. Mag. **34**, 775 (1976).